Joule

CellPress

Article

Correlating Structure and Function of Battery Interphases at Atomic Resolution Using Cryoelectron Microscopy

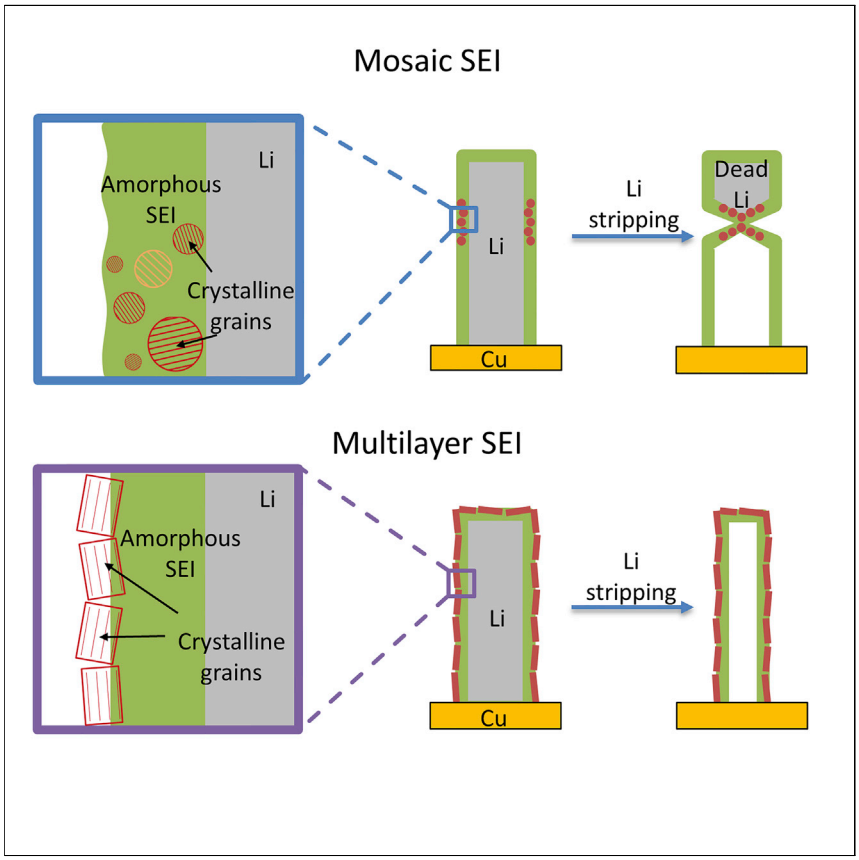

The solid electrolyte interphase (SEI) forms on all lithium battery anodes during operation and dictates their performance. Using cryoelectron microscopy, we stabilize these reactive materials for atomic-scale observation and correlate their nanostructure with battery performance. By imaging at various stages of battery operation, we reveal that the distribution of crystalline domains within the SEI is critical for the uniform transport of lithium ions. This establishes the important role that the SEI nanostructure plays in determining the performance of a battery.

Yuzhang Li, William Huang, Yanbin Li, Allen Pei, David Thomas Boyle, Yi Cui

yuzhangl@stanford.edu (Y.L.)
yicui@stanford.edu (Y.C.)

HIGHLIGHTS

Cryo-EM preserves and stabilizes Li metal anode for atomic-scale imaging

Two distinct nanostructures form on Li metal surface, dictating battery performance

Fundamental relationship between SEI nanostructure and performance is established

Ideal SEI nanostructure is critical in building efficient and safe batteries

Li et al., Joule 2, 1–11
October 17, 2018
https://doi.org/10.1016/j.joule.2018.08.004

Please cite this article in press as: Li et al., Correlating Structure and Function of Battery Interphases at Atomic Resolution Using Cryoelectron Microscopy, Joule (2018), https://doi.org/10.1016/j.joule.2018.08.004

Joule

CellPress

Article

Correlating Structure and Function of Battery Interphases at Atomic Resolution Using Cryoelectron Microscopy

Yuzhang Li,[1,4,5,*] William Huang,[1,4] Yanbin Li,[1,4] Allen Pei,[1] David Thomas Boyle,[2] and Yi Cui[1,3,*]

SUMMARY

Battery decay and failure depend strongly on the solid electrolyte interphase (SEI), a surface corrosion layer that forms on the surface of all battery electrodes. Recently, we revealed the atomic structure of these reactive and sensitive battery materials and their SEIs using cryoelectron microscopy (cryo-EM). However, the SEI nanostructure's fundamental role and effect on battery performance remain unclear. Here, we use cryo-EM to discover the function of two distinct SEI nanostructures (i.e., mosaic and multilayer) and correlate their stark effects with Li metal battery performance. We identify fluctuations in crystalline grain distribution within the SEI as the critical feature differentiating the mosaic SEI from the multilayer SEI, resulting in their distinct electrochemical stripping mechanisms. Whereas localized Li dissolution occurs quickly through regions of high crystallinity in the mosaic SEI, uniform Li stripping is observed for the more ordered multilayer SEIs, which reduces Li loss during battery cycling by a factor of three. This dramatic performance enhancement from a subtle change in SEI nanostructure highlights the importance of cryo-EM studies in revealing crucial failure modes of high-energy batteries at the nanoscale.

INTRODUCTION

Future innovations and breakthroughs in battery materials depend on our intimate understanding of their working principles and failure modes. For high-energy battery electrodes (e.g., silicon, lithium metal, sulfur), identifying critical failure points (e.g., volume expansion, dendritic growth, particle fracture, material dissolution, high reactivity) has been the key driver of materials design[1–9] and engineering solutions[10] to improving battery performance. Unfortunately, much of the current understanding has been limited to the microscale since battery materials are reactive in air[11] and easily damaged[12] from the high electron dose rates necessary for high-resolution studies. Atomic-resolution imaging of sensitive battery materials in their native states has recently been demonstrated using cryoelectron microscopy (cryo-EM), enabling new insights into nanoscale structures that have a significant impact on battery operation.[3,13]

In particular, cryo-EM revealed two distinct nanostructures of the solid electrolyte interphase (SEI), a passivation film that forms on the surface of all battery electrodes due to electrolyte decomposition.[3] The SEI plays a crucial role in battery operation,[1,2] as both electron charge transfer and Li redox reactions occur simultaneously at this interface. Although our observation resolves the longstanding debate between two prominent SEI models within the battery community, the fundamental relationship between SEI nanostructure, function, and battery performance is yet

Context & Scale

Batteries with high energy density are actively being pursued for applications in transportation and grid-level energy storage. Although high-energy battery chemistries exist, the fundamental mechanisms governing their failure modes are not well known at the atomic level. In particular, the solid electrolyte interphase (SEI) is a critical battery interface that forms on all lithium battery anodes whose exact mechanistic function is poorly understood at the atomic scale. It has been widely believed that the SEI chemistry is the major factor in regulating performance. In our present work using cryoelectron microscopy, we show for the first time that it is instead the SEI nanostructure that ultimately dictates battery performance. This surprising yet consistent finding provides an entirely new direction to explore for engineering the SEI nanostructure in battery materials.

to be established. It is this missing insight that continues to impede battery research progress, a knowledge gap we seek to fill in this work.

Indeed, this correlation between SEI nanostructure and performance is particularly important for the Li metal anode, a high-energy battery material that suffers from low coulombic efficiencies due to significant Li loss during electrochemical deposition and stripping.[14,15] Many strategies, including host architectures,[8,16,17] encapsulation,[18] conformal coatings,[19] and electrolyte additives,[20,21] have attempted to address Li metal's shortcomings by engineering the SEI layer. However, a mechanistic understanding of how and why certain strategies succeed while others fail is lacking, resulting in incremental improvement. For example, past reports have attributed improved coulombic efficiency in high-performance electrolytes to changes in SEI chemistry, converting an "unstable" or "weak" SEI layer in standard electrolytes to a "strong" and "stable" SEI layer.[22,23] Although SEI chemical composition has been probed to justify these claims,[24–26] such vague descriptions highlight our limited mechanistic understanding of performance enhancements in these electrolytes. Here, we use cryo-EM to reveal the mechanism of how different SEI nanostructures trigger failure modes in the Li metal anode, successfully correlating their structure with function for the first time. The mechanistic insight developed here suggests general design principles for engineering effective interfaces in high-energy batteries.

RESULTS AND DISCUSSION

Non-uniform Li Dissolution through Mosaic SEI

Li metal forms a mosaic SEI nanostructure when deposited in standard carbonate-based electrolyte[3] containing both ethylene carbonate (EC) and diethyl carbonate (DEC). Proposed by Peled et al., the mosaic model[27,28] suggests that organic and inorganic decomposition products from the electrolyte are precipitated and distributed heterogeneously within the SEI, forming a mosaic of microphases with both crystalline and amorphous character (Figure 1A). In contrast, Li metal forms a multilayer SEI nanostructure when deposited in the same standard carbonate-based electrolyte (EC/DEC) with an additional 10 vol% fluoroethylene carbonate[3] (FEC). In the multilayer model[29] proposed by Aurbach et al., decomposition components in the SEI are arranged uniformly to form an ordered and layered structure that separates the organic and inorganic layers (Figure 1D). Despite exhibiting a much higher coulombic efficiency in 10 vol% FEC, the Li metal deposited in this electrolyte (Figure 1E) appears to have the same dendritic morphology as that of the Li deposited in standard EC/DEC (Figure 1B). Interestingly, the electrochemically stripped Li morphology is completely different between the two electrolytes. Although the stripped Li metal in the EC/DEC electrolyte (Figure 1C) appears to have decreased in the number density but not in diameter compared with deposited Li (Figure 1B), the stripped dendrite in the 10 vol% FEC electrolyte (Figure 1F) is significantly thinner in diameter than that of the deposited Li (Figure 1E). Therefore, the SEI nanostructure may play an important role in the electrochemical stripping process.

Figure 2A shows a schematic and cryo-EM image of a typical Li metal dendrite (see Experimental Procedures) as deposited in EC/DEC. Stabilized under the cryogenic conditions in the transmission electron microscope (TEM), Li metal (low atomic number) has much lighter contrast than the carbon support film and can be identified as the vertical, rod-like structure in the center. Coated on this dendrite is a smooth and conformal film of darker contrast material, indicative of the SEI layer that contains polymeric and inorganic components (Li oxides, carbonates). High-resolution

[1]Department of Materials Science and Engineering, Stanford University, Stanford, CA 94305, USA

[2]Department of Chemistry, Stanford University, Stanford, CA 94305, USA

[3]Stanford Institute for Materials and Energy Sciences, SLAC National Accelerator Laboratory, 2575 Sand Hill Road, Menlo Park, CA 94025, USA

[4]These authors contributed equally

[5]Lead Contact

*Correspondence: yuzhangl@stanford.edu (Y.L.), yicui@stanford.edu (Y.C.)

https://doi.org/10.1016/j.joule.2018.08.004

Please cite this article in press as: Li et al., Correlating Structure and Function of Battery Interphases at Atomic Resolution Using Cryoelectron Microscopy, Joule (2018), https://doi.org/10.1016/j.joule.2018.08.004

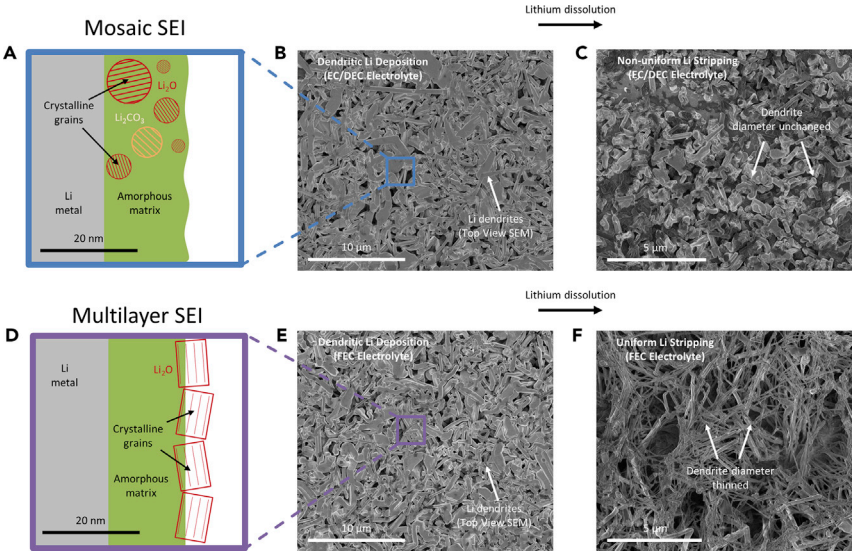

Figure 1. Li Metal Deposition and Stripping Morphology with Mosaic and Multilayer SEI Nanostructure

(A) Schematic of the mosaic SEI nanostructure that forms on Li metal in EC/DEC electrolyte. Crystalline grains are heterogeneously dispersed within a polymeric and amorphous matrix.

(B) Top-view SEM image of Li metal deposition in EC/DEC electrolyte.

(C) Top-view SEM image of stripped Li metal in EC/DEC electrolyte. Although the dendrite density appears decreased, the dendrite diameter is comparable with that of the deposited Li dendrite.

(D) Schematic of the multilayer SEI nanostructure that forms on Li metal in 10 vol% FEC electrolyte. Organic and inorganic layers are formed in an ordered structure.

(E) Top-view SEM image of Li metal deposition in 10 vol% FEC electrolyte.

(F) Top-view SEM image of stripped Li metal deposition in 10 vol% FEC electrolyte. The dendrite diameter and density are significantly decreased compared with the deposited Li dendrites.

imaging of SEI films shows their tendency to assemble into the mosaic nanostructure[3] when formed in EC/DEC electrolyte. To maximize coulombic efficiency in each battery cycle, all deposited Li metal must be completely stripped, leaving behind only the insoluble components of the SEI. This is clearly not the case for the carbonate electrolyte. Full electrochemical discharge of the deposited Li to a large overpotential of 1.0 V results in leftover Li metal still present (Figures 2B and 2D), leading to the low 88% coulombic efficiency (see Experimental Procedures). The Li metal remaining in Figures 2B and 2D is surrounded by the electrically insulating SEI, disconnecting it from the current collector and rendering the Li electrochemically inactive and "dead". Furthermore, large regions of remaining Li metal can be observed by scanning electron microscopy (SEM) after stripping to 1.0 V on the fifth cycle (Figure S1), which is also corroborated by previous reports.[30,31] Therefore, the primary failure mode in carbonate-based electrolytes is isolated and inactive Li metal. Understanding the fundamental mechanism of this inactivation process requires us to observe Li metal dendrites frozen in the middle of electrochemical stripping.

Partially stripped Li dendrites are shown in Figure 2E. Instead of fully removing the Li by electrochemically stripping to 1.0 V, we examine the dendrites after removing 50% of their original deposited capacity (see Experimental Procedures). Interestingly, notches form on the surface of the stripped dendrite as the SEI conforms to Li metal during this change in surface morphology. To form these notched structures, fast Li dissolution must be localized in these regions and occur radially around

Please cite this article in press as: Li et al., Correlating Structure and Function of Battery Interphases at Atomic Resolution Using Cryoelectron Microscopy, Joule (2018), https://doi.org/10.1016/j.joule.2018.08.004

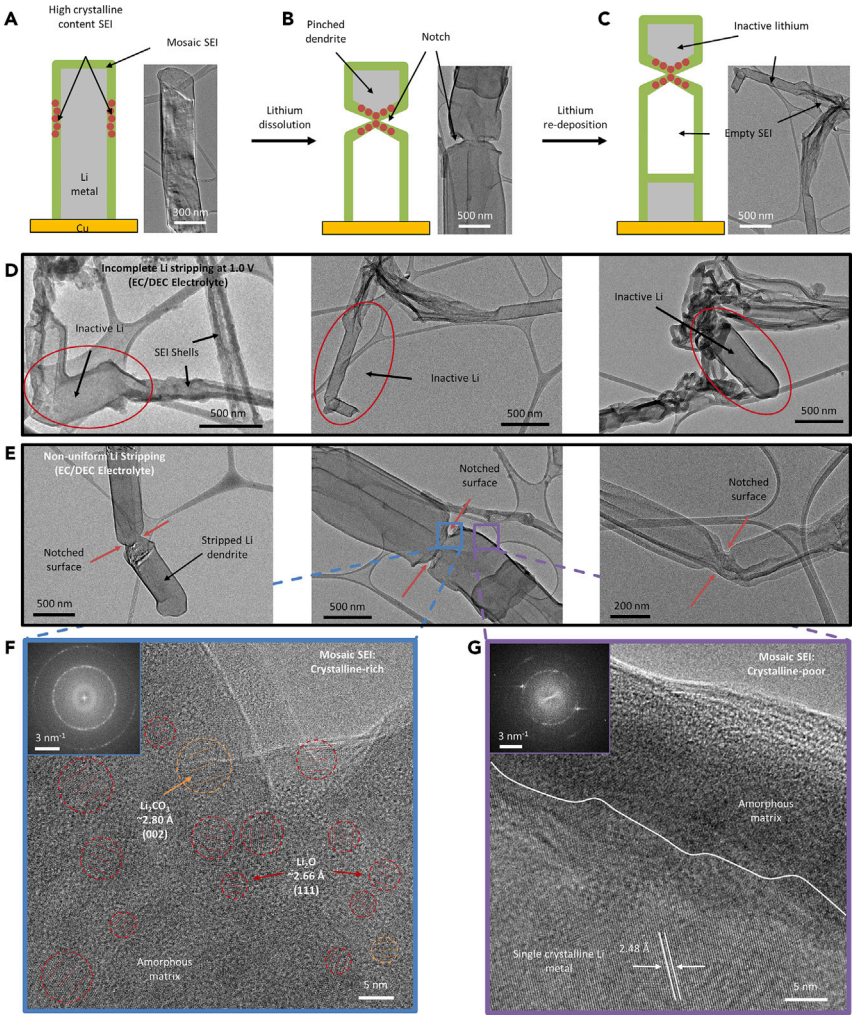

Figure 2. Non-uniform Li Stripping through Mosaic SEI

(A) Cryo-EM image and schematic of a typical Li metal dendrite formed in EC/DEC electrolyte. The dendrite surface is smooth. Electron dose rate <1 e Å^{-2} s^{-1} for ~30 s.

(B) Notched structures appear on the surface of partially stripped dendrites. Electron dose rate <1 e Å^{-2} s^{-1} for ~30 s.

(C) Electrically disconnected and electrochemically inactive Li metal remains after full electrochemical stripping to 1.0 V. Further Li metal re-deposition occurs at the current collector surface, moving the disconnected Li metal farther from the Cu current collector. Electron dose rate <1 e Å^{-2} s^{-1} for ~30 s.

(D) Additional cryo-EM images showing examples of inactive Li metal after full electrochemical stripping. Electron dose rate <1 e Å^{-2} s^{-1} for ~30 s.

(E) Additional cryo-EM images showing examples of notched surface structures on Li metal after partial electrochemical stripping. Electron dose rate <1 e Å^{-2} s^{-1} for ~30 s.

(F and G) Magnified cryo-EM images of boxed region in blue (F) and purple (G) from (E). A high concentration of crystalline grains is observed in the SEI nanostructure at the notched region, while the SEI is mostly amorphous away from the notch. Electron dose rate ~1,000 e Å^{-2} s^{-1} for ~30 s.

the dendrite perimeter. As this non-uniform stripping process continues, these notches would evolve into clefts that completely pinch off and electrically disconnect portions of Li metal in the dendrite, as seen in Figures 2B and 2D. The intimate contact between the SEI and the Li metal suggests that the SEI layer strongly governs the Li stripping process. Figure 2F shows a high-resolution cryo-EM image of the notched region, where the SEI contains mostly crystalline nanograins ~3–5 nm in

Please cite this article in press as: Li et al., Correlating Structure and Function of Battery Interphases at Atomic Resolution Using Cryoelectron Microscopy, Joule (2018), https://doi.org/10.1016/j.joule.2018.08.004

diameter. These inorganic grains of Li oxide and Li carbonate (identified by matching their lattice spacings Figure S4) are dispersed within an amorphous matrix, which is likely the organic polymer formed after electrolyte decomposition. The rings observed in the fast Fourier transform (FFT) of the high-resolution image (Figure 2F inset) suggest the SEI is rich in Li oxide, further confirming the high concentration of crystalline grains in the SEI nanostructure at the notched region. In contrast, the SEI in regions away from the notch is mostly amorphous and has low crystallinity (Figure 2G). Furthermore, the weak ring patterns in the associated FFT pattern suggests a scarcity of Li oxide grains (Figure 2G inset), with the strong diffraction spots corresponding to Li metal that appears to remain single-crystalline during stripping.

This analysis has been repeated for multiple dendrites (Figures S3 and S8). In addition to structural information, cryo-EM stabilizes the Li metal dendrites to enable elemental analysis by electron energy loss spectroscopy (EELS). Since the organic components of the SEI are decomposition products of the organic electrolyte, the carbon content is expected to be comparable with the oxygen content in an SEI region that is predominantly amorphous (Figure S9). In contrast, a highly crystalline SEI region containing Li oxide and Li carbonate grains would be expected to have a much higher oxygen content than carbon. Using scanning transmission electron microscopy coupled with EELS, we can spatially map the elemental components of Li, C, and O. Quantitative analysis of the EELS data reveals that the C to O atomic ratio is approximately 1 for regions away from the notch, indicating a largely amorphous SEI (Figures S10–S12). At the notched region, the C to atomic ratio is much lower (~0.5), further showing that this region contains a high concentration of crystalline inorganic components. These data demonstrate that the mosaic SEI nanostructure formed in EC/DEC electrolyte has a heterogeneous spatial distribution of inorganic crystalline domains along a single Li dendrite.

From these observations, we hypothesize that nanocrystalline components in the SEI facilitate fast Li ion transport through the amorphous, polymeric matrix. Such ceramic-like crystalline grains (i.e., Li oxide) are known to have low ionic conductivity in the bulk,[32] making conduction pathways more likely to proceed at the crystalline-polymer interface. Indeed, numerous reports in the literature experimentally show dramatic enhancement of ionic conductivity when ceramic nanoparticles are dispersed in solid polymer electrolytes,[33–36] a system that closely resembles the SEI layer. One proposed explanation from Wieczorek[37,38] suggests that a strong affinity exists between acidic groups on the nano-oxide surface and the anion of the Li salt in the electrolyte (PF_6^- in this case). This helps to separate the $Li^+PF_6^-$ ion pair and allow free Li ions to move rapidly at the ceramic-polymer interface. Alternatively, the rapid ionic conduction at interfaces in heterostructured materials demonstrated in many previous studies could also be attributed to space-charge effects.[39] Clearly, it is evident that the non-uniform distribution of nanocrystalline components in the SEI plays a major role in notch formation along the dendrite.

Uniform Li Dissolution through Multilayer SEI

Figure 3A shows a typical Li metal dendrite deposited in EC/DEC electrolyte with 10 vol% FEC additive. These dendrites exhibit almost identical morphologies with those deposited in the absence of FEC additive (Figure 2A). Additionally, the familiar coating on the Li dendrite exists and has a dark contrast in the cryo-EM image, indicative of the SEI layer (Figure 3A). Despite this similar deposition morphology and density, batteries using the FEC additive exhibit a dramatic improvement of the coulombic efficiency to 96% (see Experimental Procedures). This result implies that the amount of electrochemically inactive Li metal is significantly reduced in

Please cite this article in press as: Li et al., Correlating Structure and Function of Battery Interphases at Atomic Resolution Using Cryoelectron Microscopy, Joule (2018), https://doi.org/10.1016/j.joule.2018.08.004

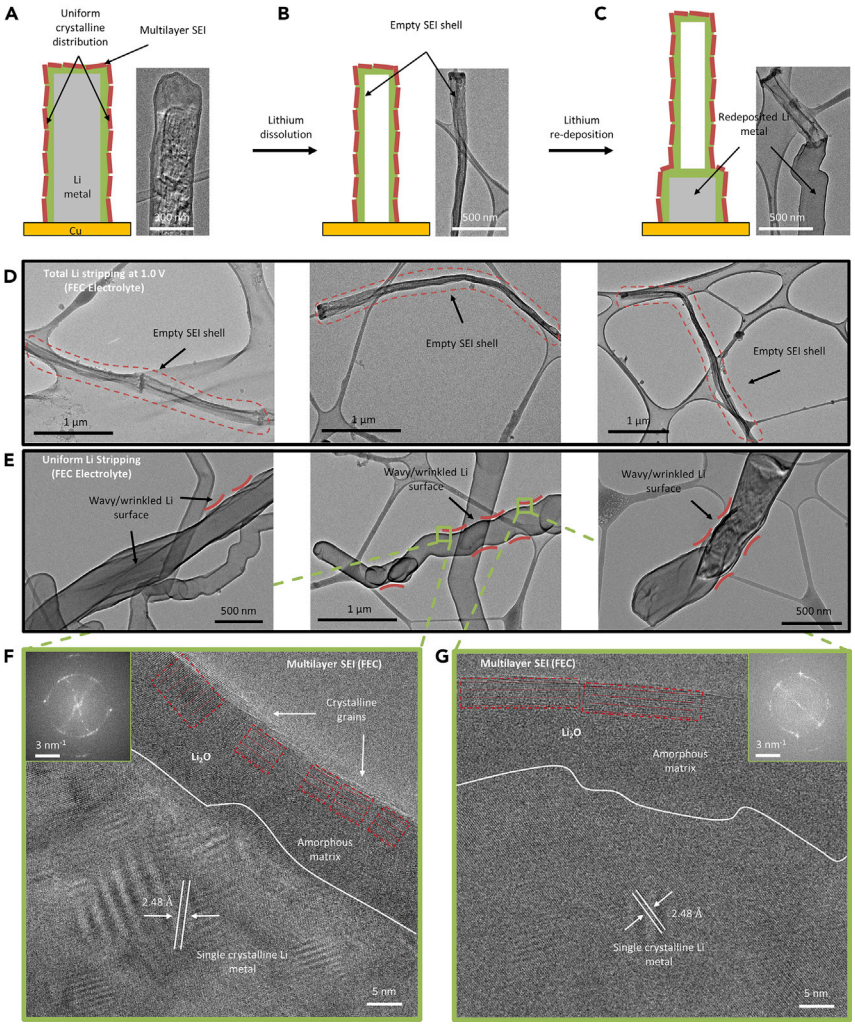

Figure 3. Uniform Li Stripping through Multilayer SEI

(A) Cryo-EM image and schematic of a typical Li metal dendrite formed in EC/DEC electrolyte with 10 vol% FEC additive. The dendrite surface is smooth, similar to dendrites formed in electrolyte without FEC additive. Electron dose rate <1 e Å^{-2} s^{-1} for ~30 s.

(B) Empty SEI shells remain after full electrochemical stripping to 1.0 V, indicating inactive Li metal is significantly reduced. Electron dose rate <1 e Å^{-2} s^{-1} for ~30 s.

(C) Redeposited Li metal pushes up the empty SEI shells away, forming new SEI on the newly deposited Li surface. Electron dose rate <1 e Å^{-2} s^{-1} for ~30 s.

(D) Additional cryo-EM images of fully stripped Li dendrites, resulting in empty SEI shells. Electron dose rate <1 e Å^{-2} s^{-1} for ~30 s.

(E) Electrochemical stripping proceeds uniformly, forming wavy structures that differ from the straight and smooth surface of as-deposited Li dendrites. Electron dose rate <1 e Å^{-2} s^{-1} for ~30 s.

(F and G) Magnified cryo-EM images of left (F) and right (G) boxed regions in green from (E). The multilayer SEI nanostructure is ordered with a homogeneous distribution of crystalline domains layered on top of the amorphous matrix. Electron dose rate ~1,000 e Å^{-2} s^{-1} for ~30 s.

the presence of FEC, with only 4% Li lost per cycle in the FEC electrolyte compared with 12% Li loss in the standard EC/DEC electrolyte. Indeed, when we electrochemically strip Li metal to 1.0 V, we observe empty SEI shells with no Li metal remaining inside (Figures 3B and 3D). With the Li metal fully removed, the empty SEI shell collapses, resulting in a wire-like morphology with a significantly thinner diameter (~50 nm) than the deposited Li metal dendrite (~300 nm). Further confirmation

with SEM images of stripped dendrites shows only empty SEI shells (Figure S2). Interestingly, partially stripped Li metal dendrites do not exhibit any notched structures on the surface (Figure 3E), as was the case in standard EC/DEC electrolyte (Figure 2E). Instead, the dendrites develop a wavy and curved morphology along the surface when Li metal is partially removed, in contrast to the more linear and straight surface for deposited Li metal (Figure 3A). This suggests that Li dissolution is more uniform through the SEI along the entire dendrite in the FEC electrolyte system.

Atomic-resolution imaging of the SEI surface by cryo-EM provides evidence for this observed difference in Li stripping behavior between standard EC/DEC electrolyte and FEC-additive electrolyte. At two different regions of the stripped dendrite, the SEI appears to have a multilayer nanostructure typical of films formed in the presence of FEC additive[3] (Figures 3F and 3G). Crystalline grains (identified to be Li oxide by matching lattice spacings) are more uniformly dispersed on top of the amorphous matrix along the dendrite in both regions. Furthermore, the FFT pattern (Figures 3F and 3G inset) and the high-resolution cryo-EM image both show that the lattices of these crystalline components are fairly aligned in the same direction. With no obvious increase in crystalline grain density within the SEI in any specific region along the dendrite, uniform Li transport can then proceed through this multilayer SEI until Li metal is fully stripped (Figures 3B and 3D). From electrochemical impedance spectroscopy, it also appears that the charge transport resistance through this multilayer SEI is lower than that of the mosaic SEI (Figure S7), further facilitating a uniform stripping process. The subtle effect of the FEC additive to change the SEI nanostructure results in a dramatic improvement in the Li metal battery performance, with the remaining loss in coulombic efficiency (4%) coming from the irreversible formation of SEI shells that are not completely refilled by Li metal during re-deposition (Figure 3C).

Simulation of Structure Change in Stripped Dendrites with Non-uniform Li Transport

Although qualitative differences in crystalline grain distribution within the mosaic and multilayer SEI nanostructure have been identified as the controlling parameter of Li transport, we still need to quantify how variations in SEI ionic conductivity affect the dendrite structure during electrochemical stripping. Figure 4A shows a COMSOL simulation of a typical Li dendrite (gray) coated with a layer of SEI (green) before stripping (see Experimental Procedures, Figure S6). We model the SEI layer as a ~30 nm film with uniform ionic conductivity along the dendrite. Furthermore, we add in a small region of increased ionic conductivity (red) in the SEI ranging four orders of magnitude. When the ionic conductivity is uniform along the SEI (Figure 4B), the Li dendrite strips evenly as expected and takes 104 s to reach 25% of its original diameter. However, when the ionic conductivity is increased beyond one order of magnitude (Figures 4D–4F), an obvious notch begins to form on the stripped dendrite at the higher conductivity defect (red), matching our previous observation (Figure 2B). With the ionic conductivity at the defect increased by three orders of magnitude (Figure 4E), the notch quickly (32 s) develops into a cleft that would pinch off the dendrite and electrically disconnect the Li metal from the current collector. Interestingly, ionic conductivity differences within an order of magnitude seem to generate curved surfaces rather than notches on the stripped dendrite (Figure 4C), closely resembling the wavy structure observed in dendrites with a multilayer SEI (Figure 3B). Therefore, uniform Li metal stripping can still occur with minor variations in ionic conductivity along the SEI, provided the differences are within an order of magnitude.

Please cite this article in press as: Li et al., Correlating Structure and Function of Battery Interphases at Atomic Resolution Using Cryoelectron Microscopy, Joule (2018), https://doi.org/10.1016/j.joule.2018.08.004

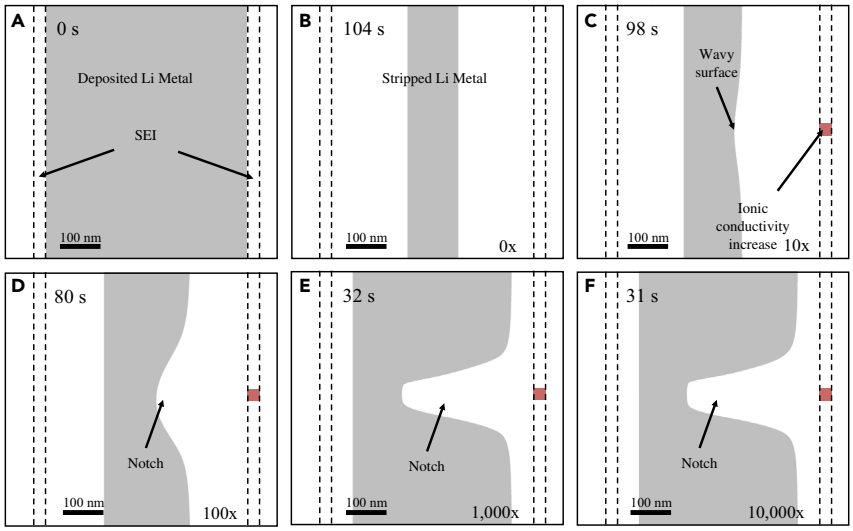

Figure 4. COMSOL Simulation of Li Dissolution through SEI Nanostructure

(A) Initial state of the modeled Li metal dendrite (500 nm diameter) with SEI layer (30 nm thick).

(B) Final structure of a stripped dendrite with uniform Li ionic conductivity through the SEI. 104 s represents the time needed to strip to 25% of the original diameter.

(C–F) Final structures of stripped dendrites with a defect (in red) introduced into the SEI with 10× (C), 100× (D), 1,000× (E), and 10,000× (F) increase in ionic conductivity. Wavy structures with curved surfaces on the stripped Li metal appear when the ionic conductivity in the defect is within 1 order of magnitude (C). Notches appear when the ionic conductivity increases beyond ~1 order of magnitude (D–F).

Conclusions

For the first time, we use cryo-EM to reveal the dynamic and fundamental effect of distinct SEI nanostructures on Li metal battery performance. Crystalline grains must be distributed evenly such that the ionic conductivity does not vary significantly both spatially and in magnitude for uniform stripping. Furthermore, the favorable multilayer SEI nanostructure found in this study opens new research questions to explore. Specifically, the unknown formation mechanism of different SEI nanostructures will be critical in providing insight for rationally designing electrolyte additives. These fundamental findings at the nanoscale enabled by cryo-EM demonstrate the exciting opportunities this powerful technique provides for battery materials research.

EXPERIMENTAL PROCEDURES

Battery Construction and Electrochemistry

In an argon-filled glovebox, type-2032 coin cells were assembled with a polymer separator (Celgard 2250), Li metal (Alfa Aesar) as the counter and reference electrode, and a Cu foil as the working electrode. The commercial electrolyte used was 1.0 M $LiPF_6$ in 1:1 w/w EC/DEC (BASF Selectilyte LP40). In experiments with electrolyte additive, 1.0 M $LiPF_6$ in 90 vol% 1:1 w/w EC/DEC with 10 vol% FEC (Novolyte Technologies) was used. All coin cells were made with ~20 μL of electrolyte volume. For Li metal deposition, a negative areal current density of 2.0 mA cm^{-2} was applied for 30 min, resulting in an areal capacity of 1.0 mAh cm^{-2} (BioLogic VMP3). For full Li metal stripping after the deposition protocol, a positive areal current density of 2.0 mA cm^{-2} was applied until the working potential reached 1.0 V. All voltages in this study are referenced versus Li metal unless otherwise stated. For partial Li metal stripping after the deposition protocol, a positive areal

current density of 2.0 mA cm^{-2} was applied for 15 min, resulting in the dissolution of ~50% of the deposited Li metal. For cryo-EM analysis, batteries were disassembled in an argon-filled glovebox. The Cu working electrode was washed briefly with 1,3-dioxolane electrolyte to remove Li salts. The remaining Li metal was removed and placed onto a lacey carbon TEM grid for analysis.

Cryo-Sample Preparation and Cryo-EM Imaging Conditions

Once the sample is placed onto the TEM grid and dried, it is quickly transferred into liquid nitrogen outside of the argon-filled glovebox using a sealed container. The sample is then placed onto the cryo-EM holder while immersed in liquid nitrogen and directly inserted into the TEM column at −170°C. A special shutter on the cryo-EM holder prevents air exposure and moisture from condensing onto the sample while any side reactions that may introduce experimental artifacts are kinetically inhibited. Unless otherwise stated, all TEM images shown in this study are taken at cryogenic temperatures (−170°C), which dramatically reduces beam damage. Sample regions were exposed to electron (*e*) dose rates of ~1,000 *e* $Å^{-2}$ s^{-1} for ~30 s in high-resolution images and <1 *e* $Å^{-2}$ s^{-1} for ~30 s in low-resolution images (details in figure captions).

Electron Microscopy

All TEM characterizations were carried out using an FEI Titan 80-300 environmental (scanning) TEM operated at 300 kV. The microscope was equipped with an aberration corrector in the image-forming (objective) lens, which was tuned before each sample analysis. All cryo-EM images were acquired with an exposure time in the range of 0.04–0.5 s using a OneView camera (Gatan). During the TEM image acquisition, the corresponding electron dose flux (measured in units of number of electrons per square angström per second, e− $Å^{-2}{\cdot}s^{-1}$) was also recorded. This parameter had been calibrated for the instrument using an analytical TEM holder with a Faraday cup. Lattice spacings of Li metal and its salts were analyzed using DigitalMicrograph (Gatan) software. SEM characterizations were carried out using an FEI Magellan 400 XHR.

Coulombic Efficiency Calculation

The average coulombic efficiency of all coin cells was evaluated for the first 10 cycles according to a modified Aurbach method.[40] This approach accurately determines the coulombic efficiency by plating and stripping Li on a Li reservoir rather than bare Cu. A 5 mAh Li reservoir was deposited and stripped to passivate the Cu surface, then the operational 5 mAh reservoir was deposited. A fixed capacity of 1 mAh was cycled 10 times at a current density of 2 mA cm^{-2}, and the Li reservoir was then fully stripped. The capacity loss in the reservoir was averaged over 10 cycles to give an accurate coulombic efficiency. The reported coulombic efficiencies of 88% in EC/DEC and 96% in FEC electrolyte are the average of three cycled cells. An example calculation and voltage profile can be found in Figure S5.

COMSOL Simulation

The simulations were performed using COMSOL Multiphysics with the physics module Tertiary Current Distribution, Nernst-Planck and the deforming mesh of the electrodeposition module. The average current through the cell was set as 2 mA cm^{-2}. The majority of the simulation cell consists of the electrolyte impregnated separator with thickness 25 μm. The diffusion coefficient of Li^+ in the electrolyte[41] was set to 3.2×10^{-6} cm^2 s^{-1}. The Li^+ diffusion coefficient in the SEI was set to 1×10^{-10} cm^2 s^{-1}. Initial Li ion concentration was set to 1.0 M.

To generate the high-conductivity region in the SEI and maintain continuity of the ionic conductivity, the diffusion coefficient of Li^+ in the polymer coatings was spatially modified following a gaussian function with full-width half-maximum 15 nm and maximum amplitude at the center of the coating (Equations 1 and 2).

$$g(y) = exp\left(\frac{-y^2}{2\sigma^2}\right) \quad \text{(Equation 1)}$$

$$\sigma = \frac{15 \times 10^{-9} m}{2\sqrt{2 \ln 2}} \quad \text{(Equation 2)}$$

The final diffusion coefficient of Li^+ in the defective SEI region (set as a 100 nm segment of the SEI) is:

$$D_{defect} = D_{SEI} + D_{max} * g(y - 3.05e - 6) \quad \text{(Equation 3)}$$

where D_{SEI} is 1×10^{-10}, D_{max} ranges from 1×10^{-10} (zero times increased conductivity in defect) to 1×10^{-6} (four orders of magnitude increased conductivity in defect), and y is the y coordinate of the defective region (varying conductivity in the y direction). The defect was placed in the center of the 6-μm-tall, 500-nm-thick Li dendrite. The SEI thickness was set to be 30 nm, according to experimental observations, and covered the entire Li dendrite and bulk electrode. The stripping electrode surface was set to the Li dendrite surface and the bulk electrode surface. The maximum mesh element size in the defect region was 1 nm.

SUPPLEMENTAL INFORMATION

Supplemental Information includes 12 figures and can be found with this article online at https://doi.org/10.1016/j.joule.2018.08.004.

ACKNOWLEDGMENTS

The authors thank Prof. B. Sinclair for fruitful discussions and insight. Yuzhang Li acknowledges the National Science Foundation Graduate Research Fellowship Program (NSF GRFP) for funding. A.P. acknowledges the support from the US Department of Defense through the National Defense Science & Engineering Graduate Fellowship (NDSEG) Program and from Stanford University through the Stanford Graduate Fellowship (SGF) Program. Y.C. acknowledges the support from the Assistant Secretary for Energy Efficiency and Renewable Energy, Office of Vehicle Technologies of the US Department of Energy under the Battery Materials Research (BMR) Program and Battery 500 Consortium Programs.

AUTHOR CONTRIBUTIONS

Yuzhang Li, W.H., Yanbin Li, and Y.C. conceived and designed the experiments. Yuzhang Li and W.H. conducted cryo-EM characterization. Yanbin Li and W.H. carried out materials synthesis and electrochemical characterization. A.P. conducted COMSOL simulations. D.T.B. conducted electrochemical impedance spectroscopy and other measurements. Yuzhang Li and Y.C. co-wrote the paper. All authors discussed the results and commented on the manuscript.

DECLARATION OF INTERESTS

The authors declare no competing interests.

Received: June 14, 2018
Revised: July 24, 2018
Accepted: August 12, 2018
Published: September 5, 2018

REFERENCES

1. Verma, P., Maire, P., and Novák, P. (2010). A review of the features and analyses of the solid electrolyte interphase in Li-ion batteries. Electrochim. Acta *55*, 6332–6341.
2. Peled, E., and Menkin, S. (2017). SEI: past, present and future. J. Electrochem. Soc. *164*, A1703–A1719.
3. Li, Y., Li, Y., Pei, A., Yan, K., Sun, Y., Wu, C.-L., Joubert, L.-M., Chin, R., Koh, A.L., and Yu, Y. (2017). Atomic structure of sensitive battery materials and interfaces revealed by cryo–electron microscopy. Science *358*, 506–510.
4. Chan, C.K., Peng, H., Liu, G., McIlwrath, K., Zhang, X.F., Huggins, R.A., and Cui, Y. (2008). High-performance lithium battery anodes using silicon nanowires. Nat. Nano *3*, 31–35.
5. Ji, X., Lee, K.T., and Nazar, L.F. (2009). A highly ordered nanostructured carbon–sulphur cathode for lithium–sulphur batteries. Nat. Mater. *8*, 500–506.
6. Wu, H., Chan, G., Choi, J.W., Yao, Y., McDowell, M.T., Lee, S.W., Jackson, A., Yang, Y., Hu, L., and Cui, Y. (2012). Stable cycling of double-walled silicon nanotube battery anodes through solid-electrolyte interphase control. Nat. Nanotechnol. *7*, 310–315.
7. Zheng, G., Lee, S.W., Liang, Z., Lee, H.-W., Yan, K., Yao, H., Wang, H., Li, W., Chu, S., and Cui, Y. (2014). Interconnected hollow carbon nanospheres for stable lithium metal anodes. Nat. Nanotechnol. *9*, 618–623.
8. Lin, D., Liu, Y., Liang, Z., Lee, H.-W., Sun, J., Wang, H., Yan, K., Xie, J., and Cui, Y. (2016). Layered reduced graphene oxide with nanoscale interlayer gaps as a stable host for lithium metal anodes. Nat. Nanotechnol. *11*, 626–632.
9. Li, Y., Yan, K., Lee, H.-W., Lu, Z., Liu, N., and Cui, Y. (2016). Growth of conformal graphene cages on micrometre-sized silicon particles as stable battery anodes. Nat. Energy *1*, 15029.
10. Wang, C.-Y., Zhang, G., Ge, S., Xu, T., Ji, Y., Yang, X.-G., and Leng, Y. (2016). Lithium-ion battery structure that self-heats at low temperatures. Nature *529*, 515.
11. Li, Y., Li, Y., Sun, Y., Butz, B., Yan, K., Koh, A.L., Zhao, J., Pei, A., and Cui, Y. (2017). Revealing nanoscale passivation and corrosion mechanisms of reactive battery materials in gas environments. Nano Lett. *17*, 5171–5178.
12. Egerton, R.F., Li, P., and Malac, M. (2004). Radiation damage in the TEM and SEM. Micron *35*, 399–409.
13. Wang, X., Zhang, M., Alvarado, J., Wang, S., Sina, M., Lu, B., Bouwer, J., Xu, W., Xiao, J., and Zhang, J.-G. (2017). New insights on the structure of electrochemically deposited lithium metal and its solid electrolyte interphases via cryogenic TEM. Nano Lett. *17*, 7606–7612.
14. Bruce, P.G., Freunberger, S.A., Hardwick, L.J., and Tarascon, J.-M. (2012). Li-O2 and Li-S batteries with high energy storage. Nat. Mater. *11*, 19–29.
15. Xu, W., Wang, J., Ding, F., Chen, X., Nasybulin, E., Zhang, Y., and Zhang, J.-G. (2014). Lithium metal anodes for rechargeable batteries. Energy Environ. Sci. *7*, 513–537.
16. Liang, Z., Lin, D., Zhao, J., Lu, Z., Liu, Y., Liu, C., Lu, Y., Wang, H., Yan, K., and Tao, X. (2016). Composite lithium metal anode by melt infusion of lithium into a 3D conducting scaffold with lithiophilic coating. Proc. Natl. Acad. Sci. USA *113*, 2862–2867.
17. Liu, Y., Lin, D., Liang, Z., Zhao, J., Yan, K., and Cui, Y. (2016). Lithium-coated polymeric matrix as a minimum volume-change and dendrite-free lithium metal anode. Nat. Commun. *7*, 10992.
18. Yan, K., Lu, Z., Lee, H.-W., Xiong, F., Hsu, P.-C., Li, Y., Zhao, J., Chu, S., and Cui, Y. (2016). Selective deposition and stable encapsulation of lithium through heterogeneous seeded growth. Nat. Energy *1*, 16010.
19. Tikekar, M.D., Choudhury, S., Tu, Z., and Archer, L.A. (2016). Design principles for electrolytes and interfaces for stable lithium-metal batteries. Nat. Energy *1*, 16114.
20. Li, W., Yao, H., Yan, K., Zheng, G., Liang, Z., Chiang, Y.-M., and Cui, Y. (2015). The synergetic effect of lithium polysulfide and lithium nitrate to prevent lithium dendrite growth. Nat. Commun. *6*, 7436.
21. Qian, J., Henderson, W.A., Xu, W., Bhattacharya, P., Engelhard, M., Borodin, O., and Zhang, J.-G. (2015). High rate and stable cycling of lithium metal anode. Nat. Commun. *6*, 6362.
22. Etacheri, V., Haik, O., Goffer, Y., Roberts, G.A., Stefan, I.C., Fasching, R., and Aurbach, D. (2011). Effect of fluoroethylene carbonate (FEC) on the performance and surface chemistry of Si-nanowire Li-ion battery anodes. Langmuir *28*, 965–976.
23. Zhang, X., Cheng, X., Chen, X., Yan, C., and Zhang, Q. (2017). Fluoroethylene carbonate additives to render uniform Li deposits in lithium metal batteries. Adv. Funct. Mater. *27*, https://doi.org/10.1002/adfm.201605989.
24. Aurbach, D., Weissman, I., Zaban, A., and Chusid, O. (1994). Correlation between surface chemistry, morphology, cycling efficiency and interfacial properties of Li electrodes in solutions containing different Li salts. Electrochim. Acta *39*, 51–71.
25. Eshkenazi, V., Peled, E., Burstein, L., and Golodnitsky, D. (2004). XPS analysis of the SEI formed on carbonaceous materials. Solid State Ionics *170*, 83–91.
26. Nie, M., Abraham, D.P., Chen, Y., Bose, A., and Lucht, B.L. (2013). Silicon solid electrolyte interphase (SEI) of lithium ion battery characterized by microscopy and spectroscopy. J. Phys. Chem. C *117*, 13403–13412.
27. Peled, E. (1979). The electrochemical behavior of alkali and alkaline earth metals in nonaqueous battery systems—the solid electrolyte interphase model. J. Electrochem. Soc. *126*, 2047–2051.
28. Peled, E., Golodnitsky, D., and Ardel, G. (1997). Advanced model for solid electrolyte interphase electrodes in liquid and polymer electrolytes. J. Electrochem. Soc. *144*, L208–L210.
29. Aurbach, D., Ein-Ely, Y., and Zaban, A. (1994). The surface chemistry of lithium electrodes in alkyl carbonate solutions. J. Electrochem. Soc. *141*, L1–L3.
30. Aurbach, D., Zinigrad, E., Cohen, Y., and Teller, H. (2002). A short review of failure mechanisms of lithium metal and lithiated graphite anodes in liquid electrolyte solutions. Solid State Ionics *148*, 405–416.
31. Lu, D., Shao, Y., Lozano, T., Bennett, W.D., Graff, G.L., Polzin, B., Zhang, J., Engelhard, M.H., Saenz, N.T., and Henderson, W.A. (2015). Failure mechanism for fast-charged lithium metal batteries with liquid electrolytes. Adv. Energy Mater. *5*, https://doi.org/10.1002/aenm.201400993.
32. Guan, P., Liu, L., and Lin, X. (2015). Simulation and experiment on solid electrolyte interphase (SEI) morphology evolution and lithium-ion diffusion. J. Electrochem. Soc. *162*, A1798–A1808.
33. Croce, F., Appetecchi, G.B., Persi, L., and Scrosati, B. (1998). Nanocomposite polymer electrolytes for lithium batteries. Nature *394*, 456–458.
34. Balazs, A.C., Emrick, T., and Russell, T.P. (2006). Nanoparticle polymer composites: where two small worlds meet. Science *314*, 1107–1110.
35. Janek, J., and Zeier, W.G. (2016). A solid future for battery development. Nat. Energy *1*, 16141.
36. Liu, W., Lee, S.W., Lin, D., Shi, F., Wang, S., Sendek, A.D., and Cui, Y. (2017). Enhancing ionic conductivity in composite polymer electrolytes with well-aligned ceramic nanowires. Nat. Energy *2*, 17035.
37. Wieczorek, W., Such, K., Wyciślik, H., and Płocharski, J. (1989). Modifications of crystalline structure of PEO polymer electrolytes with ceramic additives. Solid State Ionics *36*, 255–257.
38. Wieczorek, W., Florjanczyk, Z., and Stevens, J.R. (1995). Composite polyether based solid electrolytes. Electrochim. Acta *40*, 2251–2258.
39. Sata, N., Eberman, K., Eberl, K., and Maier, J. (2000). Mesoscopic fast ion conduction in nanometre-scale planar heterostructures. Nature *408*, 946–949.
40. Adams, B.D., Zheng, J., Ren, X., Xu, W., and Zhang, J. (2017). Accurate determination of coulombic efficiency for lithium metal anodes and lithium metal batteries. Adv. Energy Mater. *8*, 1702097.
41. Valøen, L.O., and Reimers, J.N. (2005). Transport properties of LiPF6-based Li-ion battery electrolytes. J. Electrochem. Soc. *152*, A882–A891.